

Localization Properties of Quantized Magnetostatic Modes in Nanocubes

H. Puzkarski*, M. Krawczyk

*Surface Physics Division, Faculty of Physics, Adam Mickiewicz University,
ul. Umultowska 85, Poznań, 61-614 Poland.*

J.-C. S. Lévy

*Laboratoire de Physique Théorique de la Matière Condensée, case 7020,
Université Paris 7, 2 place Jussieu, 75251 Paris Cédex 05 France.*

(Dated: November 10, 2018)

Abstract

We investigate the dynamical properties of a system of interacting magnetic dipoles disposed in sites of an sc lattice and forming a cubic-shaped sample of size determined by the cube edge length $(N - 1)a$ (a being the lattice constant, N representing the number of dipolar planes). The dipolar field resulting from the dipole-dipole interactions is calculated numerically in points of the axis connecting opposite cube face centers (*central axis*) by collecting individual contributions to this field coming from each of the N atomic planes perpendicular to the central axis. The applied magnetic field is assumed to be oriented along the central axis, magnetizing uniformly the whole sample, all the dipoles being aligned parallelly in the direction of the applied field. The frequency spectrum of magnetostatic waves propagating in the direction of the applied field is found numerically by solving the Landau-Lifshitz equation of motion including the local (*nonhomogeneous*) dipolar field component; the mode amplitude spatial distributions (*mode profiles*) are depicted as well. It is found that only the two energetically highest modes have *bulk-extended* character. All the remaining modes are of *localized* nature; more precisely, the modes forming the lower part of the spectrum are localized in the *subsurface region*, while the upper-spectrum modes are localized around the sample center. We show that the mode localization regions narrow down as the cube size, N , increases (we investigated the range of $N=21$ to $N=101$), and in sufficiently large cubes one obtains practically only *center-localized* and *surface-localized* magnetostatic modes.

PACS numbers: 75.30.Ds, 75.40.Gb, 75.75.+a

Keywords: magnetostatic modes; magnetic nanograins; mode localization; demagnetizing field

I. INTRODUCTION

The development of nanotechnology in recent years allowed to design nanometric ferromagnetic materials of any required shape with a large size variation range¹. Small magnets and particles have raised an increasing interest due to their potential application in magnetic random access memory (MRAM) elements and ultrahigh-density storage. This interest also involves the sample ability to rapidly change the magnetization state in order to optimize the individual recording time. Particularly, magnetostatic modes are of practical importance in this matter (especially in magnetization reversal processes), by reason of their low frequency range.

The small magnetic elements used in signal processing devices are of nanoscale size and mostly non-ellipsoidal shape. In such small magnetic particles the internal field non-uniformity due to the particle shape has to be taken into account. Of course, the dominant mechanism in the creation of such a nonhomogeneity are long-range dipolar interactions. The dipolar size and shape effects present in the magnetostatic wave spectra of small nonellipsoidal particles result in additional power losses² very important in device applications.

The nonuniform demagnetizing field in a normally magnetized disk was studied long ago by Yukawa and Abe³, with the assumption of uniform saturation magnetization throughout the disk. Analyzing the ferromagnetic resonance (FMR) spectrum of the magnetostatic waves in a normally magnetized YIG disk, the authors found that these waves were excited at the disk edge and propagated radially towards the disk center with increasing wave numbers.

The dynamical properties of small magnetic elements have been actively investigated recently in studies using different methods and approaches. Resonance methods combined with surface tunneling microscopy techniques enabled several teams^{4,5,6} to observe magnetostatic and exchange modes on a very local scale; time-resolved and space-resolved MOKE experiments⁷ were used to study the local magnetization dynamics as well. These different methods give good indications of the localized magnetostatic mode existence, especially when the applied field is strong enough to induce a magnetization saturation throughout the sample.

The localized magnetostatic mode dynamics has been investigated by several authors. Berkov *et al.*⁸ studied the spin wave frequency spectrum and spatial distribution in thin

μm -sized magnetic film samples. The lowest-frequency modes were found to correspond to oscillations restricted to the boundary regions, which start to ‘propagate’ inside a rectangular magnetic sample as the frequency increases. Tamaru *et al.*⁹ applied a spatially resolved FMR technique to quantized magnetostatic mode imaging in small magnetic structures. They identified quantized magnetostatic modes in the obtained spectra, and from the observed spatial distribution of magnetization response at each mode peak deduced that the number of mode nodes decreased with increasing bias field. However, in their data interpretation some discrepancies were found between the measured mode frequency values and those calculated on the basis of the Damon-Eshbach theory¹⁰. An exact theory of spin wave mode quantization in small magnetic structures needs to be developed.

The dipole-exchange spectrum of the discrete spin wave modes resulting from the bias magnetic field inhomogeneity inside a nonellipsoidal rectangular magnetic sample has been studied recently by Guslienko *et al.*¹¹. The authors found that the strong inhomogeneity of the internal bias magnetic field along the magnetization direction results in spin wave mode localization at either the edges (exchange localization) or the center (dipolar localization) of the sample. We will show in this paper that in a cubic-shaped sample with an internal field nonhomogeneity resulting solely from pure dipolar interactions these two types of magnetostatic mode localization are also present (it means magnetostatic modes are found to be localized not only at the cube center, but also on the cube surfaces).

Our theoretical approach is based on a modified Draaisma-de Jonge treatment¹² used in the dipolar energy calculation. In the original Draaisma-de Jonge treatment a ferromagnetic film is considered as a set of discrete magnetic dipoles regularly arranged in a crystalline lattice. The dipolar energy is calculated by collecting contributions from each dipolar lattice plane assumed to be parallel to the film surface. The dipoles within each plane are divided into two sets: those within a circle of radius R and those beyond that circle; the total contribution of the former set is calculated discretely through summing over the dipoles, while the contribution of the latter set is evaluated by integration (the circle radius should be large enough to assure reliable final results). In the approach used in our study, the discrete summation is performed over *all* the dipoles within a given dipolar plane; thus, the integration is avoided, and no approximation is involved in our dipolar energy evaluation.

The reason to use a discrete approach in the dipolar field calculation is our general belief¹³ that the continuous models¹⁰ used in deriving magnetostatic modes become rather

questionable when applied to small samples containing a finite number of elementary spins. The complexity of introducing the long-range spin-spin interactions into the discrete approach is balanced by the restriction of our study only to the case of a uniform mode within each dipolar plane, which reduces the 3D problem to a single dimension (this assumption is experimentally justified by the observed weak in-plane variability of the magnetic modes¹⁴).

II. A FINITE SYSTEM OF MAGNETIC DIPOLES IN PLANAR ARRANGEMENT

We shall consider a system of magnetic moments $\mu_{\vec{r}}$ arranged regularly in sites \vec{r} of a simple cubic crystal lattice. The system is assumed to form a rectangular prism with square base (see Fig. 1a). Let the prism base determine the (x, y) -plane of a Cartesian reference system, with the z -axis perpendicular to this plane. The reference point $(0, 0, 0)$ shall be placed in the *central* site of the prism bottom.

Let us calculate magnetic field $\vec{h}_{\vec{R}}$ "produced" by all the prism dipoles in a site indicated by internal vector \vec{R} . According to the classical formula (obtained using the linear approximation¹⁵), field $\vec{h}_{\vec{R}}$ can be expressed as follows (in the SI units):

$$\vec{h}_{\vec{R}} = \frac{1}{4\pi} \sum_{\vec{r} \neq \vec{R}} \frac{3(\vec{r} - \vec{R}) (\vec{\mu}_{\vec{r}} \cdot (\vec{r} - \vec{R})) - \vec{\mu}_{\vec{r}} |\vec{r} - \vec{R}|^2}{|\vec{r} - \vec{R}|^5}, \quad (1)$$

the above sum involving all the sites *except* the reference point (*i.e.* the site with position vector $\vec{r} \equiv \vec{R}$). The lattice planes parallel to the prism base shall be numbered with index $n \in \langle 0, N - 1 \rangle$ (see Fig. 1b), and the sites within each plane indexed with vector $\vec{r}_{||} = a[p\hat{i} + q\hat{j}]$, defined by integers $p, q \in \langle -L, L \rangle$. This means that the position of the sites in which the magnetic moments are located, indicated by vector \vec{r} , shall be defined by a set of three integers, (p, q, n) :

$$\vec{r} \equiv [\vec{r}_{||}, an] \equiv a[p, q, n], \quad p, q \in \langle -L, +L \rangle \quad \text{and} \quad n \in \langle 0, N - 1 \rangle, \quad (2)$$

a denoting the lattice constant. Thus, the considered prism contains $N(2L + 1)^2$ magnetic moments. Below we shall focus on the magnetic field on the z -axis only, assuming its direction to be solely allowed for magnetic wave propagation. Hence, we put $\vec{R} \equiv a[0, 0, n']$, where $n' \in \langle 0, N - 1 \rangle$, and re-index the dipole field: $\vec{h}_{n'} \equiv \vec{h}_{\vec{R}}$. By vector decomposition:

$$\vec{r} - \vec{R} = a(p\hat{i} + q\hat{j} + (n - n')\hat{k}), \quad (3)$$

equation (1) becomes :

$$\begin{aligned}
\vec{h}_{\vec{R}} &\equiv \vec{h}_{\vec{n}'} = \frac{1}{4\pi} \sum'_{p,q,n} \left[\frac{3a(p\hat{i} + q\hat{j} + (n-n')\hat{k}) (\vec{\mu}_{\vec{r}} \cdot a(p\hat{i} + q\hat{j} + (n-n')\hat{k}))}{(a\sqrt{p^2 + q^2 + (n-n')^2})^5} \right. \\
&\quad \left. - \frac{\vec{\mu}_{\vec{r}} a^2 (p^2 + q^2 + (n-n')^2)}{(a\sqrt{p^2 + q^2 + (n-n')^2})^5} \right] \\
&= \frac{1}{4\pi} \sum'_{p,q,n} \left[3 \frac{\hat{i}(\mu_{\vec{r}}^x p^2 + \mu_{\vec{r}}^y pq + \mu_{\vec{r}}^z p(n-n')) + \hat{j}(\mu_{\vec{r}}^x pq + \mu_{\vec{r}}^x q^2 + \mu_{\vec{r}}^z q(n-n'))}{a^3(p^2 + q^2 + (n-n')^2)^{\frac{5}{2}}} \right. \\
&\quad + \frac{3\hat{k}(\mu_{\vec{r}}^x p(n-n') + \mu_{\vec{r}}^y q(n-n') + \mu_{\vec{r}}^z (n-n')^2)}{a^3(p^2 + q^2 + (n-n')^2)^{\frac{5}{2}}} \\
&\quad \left. - \frac{(\mu_{\vec{r}}^x \hat{i} + \mu_{\vec{r}}^y \hat{j} + \mu_{\vec{r}}^z \hat{k})(p^2 + q^2 + (n-n')^2)}{a^3(p^2 + q^2 + (n-n')^2)^{\frac{5}{2}}} \right], \quad (4)
\end{aligned}$$

the triple sum over indices p, q, n ($\sum_{\vec{r}} \equiv \sum_{n,p,q}$) replacing the single sum over vectors \vec{r} ; the summing range is as defined in (2), and the prime (') at the sum symbol means that the reference point $[0, 0, n']$ is excluded from the sum. As the site distribution within each plane n is symmetric with respect to site $(0, 0, n)$, each site (p, q) has its counterpart $(-p, -q)$. Consequently, in sum (4), all the terms in which p and q appear in odd powers are compensated, and (4) becomes:

$$\begin{aligned}
\vec{h}_{n'} &= \frac{1}{4\pi} \sum'_{p,q,n} \left[3 \frac{\hat{i}\mu_{\vec{r}}^x p^2 + \hat{j}\mu_{\vec{r}}^y q^2 + \hat{k}\mu_{\vec{r}}^z (n-n')^2 - \hat{i}\mu_{\vec{r}}^x (p^2 + q^2 + (n-n')^2)}{a^3(p^2 + q^2 + (n-n')^2)^{\frac{5}{2}}} \right. \\
&\quad \left. - \frac{\hat{j}\mu_{\vec{r}}^y (p^2 + q^2 + (n-n')^2) + \hat{k}\mu_{\vec{r}}^z (p^2 + q^2 + (n-n')^2)}{a^3(p^2 + q^2 + (n-n')^2)^{\frac{5}{2}}} \right] \\
&= \frac{1}{4\pi} \sum'_{p,q,n} \left[\frac{\hat{i}\mu_{\vec{r}}^x (2p^2 - q^2 - (n-n')^2) + \hat{j}\mu_{\vec{r}}^y (-p^2 + 2q^2 - (n-n')^2)}{a^3(p^2 + q^2 + (n-n')^2)^{\frac{5}{2}}} \right. \\
&\quad \left. + \frac{\hat{k}\mu_{\vec{r}}^z (-p^2 - q^2 + 2(n-n')^2)}{a^3(p^2 + q^2 + (n-n')^2)^{\frac{5}{2}}} \right]. \quad (5)
\end{aligned}$$

Further calculations shall be performed using double sums over p and q , defined as follows:

$$I_{n,n'} = \sum'_{p,q} \frac{(n-n')^2}{[p^2 + q^2 + (n-n')^2]^{\frac{5}{2}}} \quad (6)$$

and

$$J_{n,n'} = \sum'_{p,q} \frac{p^2}{[p^2 + q^2 + (n-n')^2]^{\frac{5}{2}}} \equiv \sum'_{p,q} \frac{q^2}{[p^2 + q^2 + (n-n')^2]^{\frac{5}{2}}}$$

$$\equiv \frac{1}{2} \sum'_{p,q} \frac{p^2 + q^2}{[p^2 + q^2 + (n - n')^2]^{\frac{5}{2}}}; \quad (7)$$

the equality of the two first sums in (7) is a consequence of the fact that the z -axis is a fourfold symmetry axis for each lattice plane (see Fig. 1). Additionally, we shall assume that all the magnetic moments within a *single plane* n are identical, *i.e.*:

$$\vec{\mu}_n \equiv \vec{\mu}_{[p,q,n]}, \quad \text{for any } p \text{ and } q. \quad (8)$$

By including relations (6-8) into (5), magnetic field $\vec{h}_{n'}$ can be expressed as follows:

$$\vec{h}_{n'} = \frac{1}{4\pi} \sum_n \left[(J_{n,n'} - I_{n,n'}) \frac{\hat{i}\mu_n^x + \hat{j}\mu_n^y - 2\hat{k}\mu_n^z}{a^3} \right]. \quad (9)$$

Note that by assuming $\vec{\mu}_n \equiv \vec{\mu}_{\vec{r}}$ all the magnetic excitations propagating in *plane* (x, y) are excluded from our analysis, and z axis becomes the only direction of propagation allowed.

In order to obtain a simpler expression of $\vec{h}_{n'}$ we introduce a symmetric matrix whose elements, $D_{n,n'}$, are defined as follows:

$$D_{n,n'} \equiv J_{n,n'} - I_{n,n'} = \sum'_{p,q} \frac{\frac{1}{2}(p^2 + q^2) - (n - n')^2}{[p^2 + q^2 + (n - n')^2]^{\frac{5}{2}}}. \quad (10)$$

With this matrix, the magnetic field reads:

$$\vec{h}_{n'} = \frac{1}{4\pi} \sum_n \left[D_{n,n'} \frac{\hat{i}\mu_n^x + \hat{j}\mu_n^y - 2\hat{k}\mu_n^z}{a^3} \right]. \quad (11)$$

It is convenient to introduce here the notion of *magnetization*, a phenomenological quantity, which in the considered case of simple cubic lattice can be defined as follows:

$$\vec{M}_n = \vec{\mu}_n / a^3. \quad (12)$$

Then, (11) becomes:

$$\vec{h}_{n'} = \frac{1}{4\pi} \sum_n D_{n,n'} \left[\hat{i}M_n^x + \hat{j}M_n^y - 2\hat{k}M_n^z \right]. \quad (13)$$

It should be remembered that site $(0, 0, n')$ is excluded from the sums appearing in the equation (10); to avoid any ambiguity, this shall be noted explicitly by rewriting (13) in its expanded form:

$$\begin{aligned} \vec{h}_{n'} = \frac{1}{4\pi} \sum_{n \neq n'} \sum_{p,q} \frac{\frac{1}{2}(p^2 + q^2) - (n - n')^2}{[p^2 + q^2 + (n - n')^2]^{\frac{5}{2}}} \left[\hat{i}M_n^x + \hat{j}M_n^y - 2\hat{k}M_n^z \right] \\ + \frac{1}{8\pi} \sum'_{p,q} \frac{1}{[p^2 + q^2]^{\frac{3}{2}}} \left[\hat{i}M_{n'}^x + \hat{j}M_{n'}^y - 2\hat{k}M_{n'}^z \right]. \end{aligned} \quad (14)$$

The second term on the right of Eq. (14) has been calculated for $n = n'$, and thus site $\vec{r}_{||} = (0, 0)$ should be excluded from the sum over p and q (as indicated by the prime at the sum symbol). Equation (10), defining elements $D_{n,n'}$, can be interpreted as the definition of a *dipolar* matrix \hat{D} composed of these elements; as we shall see this matrix shall play an important role in deducing properties of magnetic modes. As a consequence of (10) matrix \hat{D} is symmetric, *i.e.* $D_{n,n'} \equiv D_{n',n}$. Let us introduce a new variable, defined as follows:

$$\delta = n - n'; \quad (15)$$

δ measures the distance between planes n and n' . Consequently, we can write:

$$D_{n,n'} \equiv D_{\delta} = D_{n',n} \equiv D_{-\delta}; \quad (16)$$

$$D_{\delta} = \sum'_{p,q} \frac{\frac{1}{2}(p^2 + q^2) - \delta^2}{[p^2 + q^2 + \delta^2]^{\frac{5}{2}}}. \quad (17)$$

Note that the considered system consists of a finite number of planes (index n taking values $n = 0, 1, 2, \dots, N - 1$), so the set of values available to δ depends on the reference plane, n' , with respect to which the distance is measured. However, the following condition must always be satisfied:

$$0 \leq n' + \delta \leq N - 1. \quad (18)$$

A sum over *all* the system planes shall be in use below; this sum shall be denoted as:

$$\sum_{\delta}^{n'}, \quad (19)$$

superscript n' indicating that the summing is performed on the planes neighbouring with n' , including plane n' . Therefore, δ takes the following values:

$$\delta = 0, \pm 1, \pm 2 \dots \quad (20)$$

its lower and upper limits being determined by condition (18).

Up to now, the direction of dipole arrangement has not had much importance in our reasoning. Now we shall consider the case with dipoles arranged along the z -axis only.

III. MAGNETIC DIPOLES ALIGNED ALONG THE DIRECTION OF MAGNETOSTATIC MODE PROPAGATION

In this paragraph we shall consider a magnetic prism placed in a static magnetic field, H_0 , applied along the z -axis (Fig. 1). Field H_0 is assumed to be strong enough to arrange

all the magnetic moments along the z -axis. Then, the magnetization vector can be regarded as a superposition of two components (Fig. 1): static (parallel to the z -axis) and dynamic (lying in the (x, y) -plane):

$$\vec{M}_{\vec{R}} = M_S \hat{k} + \vec{m}_{\vec{R}}; \quad (21)$$

M_S is the static magnetization, assumed to be homogeneous throughout the sample, and vector \vec{m} denotes the dynamic magnetization, perpendicular to \vec{M}_S . Similarly, the dipole field, $\vec{h}_{n'}$, can be resolved into two components: static, $\vec{h}_{n'}^s$ (parallel to the z -axis), and dynamic, $\vec{h}_{n'}^d$ (lying in the (x, y) -plane):

$$\vec{h}_{n'} = \vec{h}_{n'}^s + \vec{h}_{n'}^d. \quad (22)$$

These two components of the dipole field can be easily found from (13). By replacing the third component of the magnetization vector with the static magnetization (*i.e.* by putting $M_n^z \equiv M_S$), and the two other components, M_n^x and M_n^y , with the respective components of the dynamic magnetization, m_n^x and m_n^y , the following formulae are obtained:

$$\vec{h}_{n'}^s = - \left[\frac{1}{2\pi} \sum_n D_{n,n'} \right] M_S \hat{k}, \quad (23)$$

$$\vec{h}_{n'}^d = \frac{1}{4\pi} \sum_n D_{n,n'} \vec{m}_n, \quad (24)$$

element $D_{n,n'}$ being defined by (10).

The magnetic moment dynamics is described by the phenomenological Landau-Lifshitz equation (LL):

$$\frac{\partial \vec{M}_{\vec{R}}}{\partial t} = \gamma \mu_0 \vec{M}_{\vec{R}} \times \vec{H}_{eff, \vec{R}}, \quad (25)$$

$\vec{H}_{eff, \vec{R}}$ denoting the effective magnetic field acting on the magnetic moment in site \vec{R} . This effective field is a superposition of two terms only: the applied field, \vec{H}_0 , and the field $\vec{h}_{n'}$ produced by the magnetic dipole system:

$$\vec{H}_{eff, \vec{R}} \equiv \vec{H}_{eff, n'} = \vec{H}_0 + \vec{h}_{n'}. \quad (26)$$

Considering (22), we can write further:

$$\vec{H}_{eff, n'} = (H_0 + h_{n'}^s) \hat{k} + \vec{h}_{n'}^d; \quad (27)$$

the above-introduced dipole field components (static and dynamic) being defined by (23) and (24).

The LL equation becomes:

$$\frac{\partial \vec{m}_{n'}}{\partial t} = \gamma \mu_0 \left(M_S \hat{k} + \vec{m}_{n'} \right) \times \left((H_0 + h_{n'}^s) \hat{k} + \vec{h}_{n'}^d \right). \quad (28)$$

We shall solve it using the linear approximation, *i.e.* neglecting all the terms with \vec{m} squared. Assuming the standard harmonic time-dependence of the solutions: $\vec{m}_{n'} \sim e^{-i\omega t}$, (28) becomes:

$$-i\omega \vec{m}_{n'} = \gamma \mu_0 \left[M_S \hat{k} \times \vec{h}_{n'}^d + \vec{m}_{n'} \times (H_0 + h_{n'}^s) \hat{k} \right] \quad (29)$$

or, using the properties of vector product:

$$-i\omega \vec{m}_{n'} = \gamma \mu_0 \hat{k} \times \left[M_S \vec{h}_{n'}^d - \vec{m}_{n'} (H_0 + h_{n'}^s) \right]. \quad (30)$$

Through replacing the dipole field dynamic and static components with their explicit expressions (23) and (24) we obtain:

$$-i\omega \vec{m}_{n'} = \gamma \mu_0 \hat{k} \times \left[M_S \frac{1}{4\pi} \sum_n D_{n,n'} \vec{m}_n - \vec{m}_{n'} \left(H_0 - \frac{M_S}{2\pi} \sum_n D_{n,n'} \right) \right], \quad (31)$$

or, after bilateral multiplication by $-4\pi(\gamma\mu_0 M_S)^{-1}$:

$$i\Omega \vec{m}_{n'} = \hat{k} \times \left[\vec{m}_{n'} \left(\Omega_H - 2 \sum_n D_{n,n'} \right) - \sum_n D_{n,n'} \vec{m}_n \right], \quad (32)$$

Ω and Ω_H denoting the *reduced frequency* and the *reduced field*, respectively, defined as follows:

$$\Omega \equiv \frac{4\pi\omega}{\gamma\mu_0 M_S} \quad \text{and} \quad \Omega_H \equiv \frac{4\pi H_0}{M_S}. \quad (33)$$

Two complex variables are now introduced for convenience:

$$m_n^\pm = m_n^x \pm im_n^y; \quad (34)$$

with these new variables, (32) splits into two independent *identical* scalar equations for m_n^+ and m_n^- ; this means we are dealing with magnetostatic waves polarized *circularly*. Therefore, it is enough to consider only one of these two equations, *e.g.* that for m_n^+ :

$$\Omega m_{n'}^+ = m_{n'}^+ \left(\Omega_H - 2 \sum_n D_{n,n'} \right) - \sum_n D_{n,n'} m_n^+. \quad (35)$$

The above equation can be rewritten as follows:

$$\Omega m_{n'}^+ = m_{n'}^+ \left(\Omega_H - 2 \sum_n D_{n,n'} - D_{n',n'} \right) - \sum_{n \neq n'} D_{n,n'} m_n^+. \quad (36)$$

Matrix elements $D_{n,n'}$ mean elements of the dipolar matrix discussed in Section II; with notations introduced there, the equation (36) becomes:

$$\Omega m_{n'}^+ = m_{n'}^+ \Omega_{n'} - \sum_{\delta=1,2,\dots} D_{\delta} m_{n' \pm \delta}^+, \quad (37)$$

where we introduced the following abbreviation denoting *the local field*:

$$\Omega_{n'} \equiv \Omega_H - D_0 - 2 \sum_{\delta=0}^{n'} D_{\delta}. \quad (38)$$

It is also convenient to introduce at this stage *the reduced static demagnetizing field* - on the analogy of the reduced external field (33) - by using the definition (23):

$$\Omega_{n'}^s \equiv \frac{4\pi}{M_S} h_{n'}^s = -2 \sum_n D_{n,n'} \equiv -2 \sum_{\delta=0}^{n'} D_{\delta}. \quad (39)$$

This allows us to rewrite Eq. (38) in the form:

$$\Omega_{n'} = \Omega_H + \Omega^d + \Omega_{n'}^s, \quad (40)$$

with $\Omega^d \equiv -D_0$ and $\Omega_{n'}^s$ meaning the (*reduced*) contributions to the local field coming, respectively, from the dynamical and statical parts of the demagnetizing field. Note that, according to the assumption made at the beginning of this paragraph, the eigenvalues Ω (being reduced frequencies) correspond to magnetostatic waves propagating in the direction of the applied field, *i.e. along the central axis* shown in Fig. 2.

In the remaining part of our work we will be considering only the cubic-shaped samples, *i.e.* starting from this point we always assume $2L \equiv N - 1$. We also assume particular values for $\mu_0 H_0 = 0.2T$ and $M_S = 0.139 \cdot 10^6 Am^{-1}$ (YIG magnetization) with resulting value for the reduced field $\Omega_H = 14.374$. However, we have to emphasize that selection of this particular value for Ω_H is not essential for results to be presented in subsequent sections of this work, since the distribution of eigenvalues Ω and profiles of modes associated with them are not sensitive to the choice of particular Ω_H value: the particular value of Ω_H only sets the *whole* spectrum in a given frequency region and if Ω_H changes the whole spectrum is shifted to another region, but the *relative* distribution of mode eigenfrequencies remains unchanged.

IV. MODE FREQUENCIES AND AMPLITUDE PROFILES ALONG THE CUBE CENTRAL AXIS

We shall investigate magnetostatic excitations in a cube of size $40a$ (a being the lattice constant). Fig. 2 shows this cube in a reference system rotated by 90° with respect to that indicated in Fig. 1 (the z -axis, along which the atomic planes are counted, is now horizontal). The cube consists of 41 planes normal to the z -axis and numbered with index n , ranging from $n=0$ (the left face) to $n=40$ (the right face). The effective dipole field calculation procedure applied in the previous paragraphs allows to find the field in z -axis points only, *i.e.* along the cube *central axis*, passing through opposite cube face centers; this is the idea of the approximation used throughout this study, and henceforth referred to as *central-axis approximation (CAA)*.

The whole sample is assumed to be magnetized uniformly (the corresponding magnetization value being M_S) and in the direction of the external field, applied along the z -axis. The z -axis direction shall be also the only one allowed for propagation of the magnetostatic waves studied in this paper. With these assumptions, the problem of motion – to be solved on the basis of (25) – reduces to a single dimension in the space of variable n ; the domain of the investigated motion is the interval $n \in (0, N - 1)$, between two opposite cube face centers (Fig. 2 shows this interval in close-up).

Fig. 3 presents the discrete spectra of numerically calculated magnetostatic mode frequencies in a cube of variable size; the spectrum evolution with increasing N , or cube size, is visualized by the depicted frequency branches, each corresponding to one mode of a fixed number m . The plot shows clearly that only in the lowest N value range ($N < 50$) the frequency spectrum changes in a significant way; above this range, the frequency values stabilize at levels independent of N . A striking feature is that the frequencies of the two highest modes, $m = N-1$ and $m = N$, as well as those of the two lowest ones, $m = 1$ and $m = 2$, are pronouncedly separated from the rather uniform „band” formed by the other mode frequencies. In Fig. 4, showing all mode profiles in a $40a \times 40a \times 40a$ cube, these “detached” modes reveal quite distinct amplitude distributions, differing from those of the other modes: modes $m = N - 1$ and $m = N$ appear to be of the *bulk-extended (BE)* type (with anti-symmetrical and symmetrical amplitude distribution, respectively), whereas modes $m = 1$ and $m = 2$ are *surface-localized (SL)*, the lower one being *antisymmetrical*, and the higher

one *symmetrical*. Besides, note that the amplitude arrangement is *ferromagnetic* in the BE modes, and *antiferromagnetic* in the SL modes. All the other modes, within the „band”, can be qualified as *localized* (L), their maximum amplitudes localizing in some specific regions inside the sample; as these localization regions are found to vary with the mode number, the mode localization appears to depend on the mode frequency.

To examine this relation in detail, let’s note that the band modes can be divided into two groups: modes $m = 3 \div 24$ and $m = 25 \div 39$, showing different localization regions. A characteristic feature of the first-group modes is a zone of *zeroing* amplitudes around the sample center; *two* non-zero amplitude regions are present at both sides of the central “dead” zone. Each of these non-zero regions can be divided further into two sub-regions: an outer one, situated at the border, with ferromagnetic arrangement of the amplitudes which fade towards the sample borders, and an inner sub-region, with mostly antiferromagnetic arrangement of the amplitudes, reaching a maximum at a certain point. It is apparent from Fig. 4b that the “ferromagnetic tail” extends as the mode energy increases, shifting the neighbouring localization region inside the sample; finally the localization reaches the sample center, the modes entering the other group (*i.e.* $m = 25 \div 39$). Typical for this group, the central localization region tightens around the sample center as mode energy increases. With respect to the above-discussed localization properties in both groups, the second-group modes can be qualified as *center-localized* (CL), and the first-group ones as *non-central bulk-localized* ($NCBL$) (or, alternatively, *empty-center bulk localized*).

V. TWO TYPES OF MODE LOCALIZATION: SURFACE-LOCALIZED AND BULK-LOCALIZED MODES

Let’s study in detail the NCBL mode properties. An extremely interesting feature of this group is both amplitude and energy double degeneration, appearing simultaneously. This effect is illustrated in Fig. 5, showing the mode profiles divided into two groups: symmetrical modes (S) are separated from antisymmetrical ones (AS) (for simplicity reasons, only $|m^+|$ profiles are depicted). Note that the profiles of consecutive mode pairs: $m=1$ (AS) and $m=2$ (S), $m=3$ (AS) and $m=4$ (S), and so on are *identical*. This amplitude degeneration in AS-S mode pairs takes place throughout the whole NCBL group, to pair $m=23;24$ inclusive. Its disappearance above this pair is easy to explain: as by definition, in antisymmetrical

modes amplitude vanishes in the sample center, a necessary condition for their symmetrical counterparts to have identical amplitude distribution is a similar amplitude zeroing in the center; but this occurs in NCBL modes only. The amplitude degeneration is associated with that of energy levels; a double energy level degeneration in the NCBL group is apparent in Fig. 6. (When studying Fig. 6, note once more that the two highest modes, $m = N-1$ and especially $m = N$, are apparently separated from the other mode energy levels.)

Getting back to Fig. 5, note that all the modes have two ferromagnetic tails at their borders; the extent of these tails depends on mode frequency. In both the symmetrical and the antisymmetrical mode groups, the highest-energy mode consists of two *complete* ferromagnetic tails, each extending from a sample border to the sample center. In the highest-energy symmetrical mode, $m = N$, the tails meet in the center with their maximum amplitudes; in the counterpart antisymmetrical mode, $m = N-1$, the tails meet in the center with their zero amplitudes. An interesting thing to note is that each of these two highest modes can be regarded as the „source” of a mode family formed by all the other modes within the given symmetry group. The generation of the lower modes from the initial BE modes, $m = N$ or $m = N-1$, is based on ferromagnetic tail shrinking: receding from the sample center, the tails give way to the formation of a new mode segment, with amplitudes localized in the center (CL modes). The central localization zone broadens as energy decreases, to split into two separate (right and left) localization sub-zones, which migrate towards the borders following the continuously shrinking ferromagnetic tails. No more non-zero amplitudes appear in the vacated center, which therefore remains “dead”; this corresponds to the formation of NCBL modes. When the non-zero amplitudes reach the borders (which occurs in the lowest-frequency modes), the entire inside is dead, and the corresponding modes are of surface-localized nature.

VI. SIZE-INDUCED LOCALIZATION EFFECT

Let’s increase the cube size to examine its effect on the mode energy spectrum and profiles. Fig. 6b shows a discrete mode frequency distribution calculated for a cube of size $2L=100$; this distribution can be compared to that obtained for a cube of size $2L=40$, shown in Fig. 6a. Besides the obvious increase in the density of states (resulting from the sample enlargement), the larger cube retains the basic characteristics observed in the smaller cube,

namely: the double degeneration in the lower-spectrum modes, its absence in the upper modes, and the outstanding of the two highest modes. Note that also the mode frequency range remains virtually unchanged, and that with the increased density of states, the linear character of the mode frequency *vs.* mode number dependence is more apparent.

However, this “invariance” of the energy spectrum does not translate into the amplitude profiles. Fig. 7 presents a juxtaposition of profiles of the five lowest modes and the six highest ones in cubes of two different sizes: $2L=40$ and $2L=100$. The profile invariance is found to be limited to the BE modes only ($m=1;2$) whose profiles remain unchanged in spite of the size increase. The other states reveal apparently changed localization: the NCBL modes in the $2L=100$ cube, showing substantially larger dead regions (with respect to the $2L=40$ cube), are practically of *sub-surface localized* (SSL) nature; in the CL modes, the localization zone has tightened around the strict sample center. Thus, we can anticipate that further size increase shall result in a deepening of the above-mentioned localization changes, and that consequently, the magnetostatic mode spectrum in large cubic samples shall consist of three clearly different mode groups: (a) two highest-frequency *bulk-extended modes* (AS and S), (b) *center-localized modes* with intermediate frequencies, and (c) lowest-frequency *surface-localized modes*. Another way of illustration of this *size-induced localization effect* is given on the Fig. 8.

VII. INTERNAL DIPOLAR FIELD NONHOMOGENEITY AS THE SOURCE OF MODE LOCALIZATION

Obviously, we would like to understand why almost all of the modes forming the magnetostatic spectrum (except for the two highest ones) are of localized nature. We can suppose that this property is due to the long-range character of dipole interactions, as the latter as known to produce spatially nonhomogeneous demagnetization field in bounded non-ellipsoid systems¹⁶. In fact, this is the case of the cube considered in this paper: plotted with bold line in Fig. 9, the local field Ω_n , given by Eq.(38), shows nonhomogeneous spatial distribution (along the central axis), reaching a maximum in the sample center, and fading symmetrically towards the borders. The magnetostatic mode profiles, plotted in the same energy scale, have been superimposed on this local field plot. Strikingly, the shape of the suppressed amplitude area in the bulk resembles exactly that of the nonhomogeneous distribution of

Ω_n , and all the NCBL mode frequencies lie within the local field value range. The CL mode frequencies coincide with the top of the Ω_n curve, *i.e.* the region where the local field gradient is highest. The BE mode frequencies lie *above* the Ω_n value range, and one can think that this is why they are hardly sensitive to the local field variations.

VIII. FINAL REMARKS AND OUTLOOKS

In their recently performed systematic studies of FMR in patterned submicron rectangular permalloy films, Zhai *et al.*¹⁷ observed multippeak spectra interpreted as spin-wave resonance due to the non-uniform magnetization of the studied samples. We expect a similar study can be performed on cubic structures as well, with the aim of revealing different types of the above-described localized modes.

One of the practical aspects of our study concerns the size-independence of magnetostatic mode frequencies found in cubic-shaped samples. This is in contrast with the recent report¹⁸, where FMR spectra were measured for a series of single crystal yttrium-iron-garnet (YIG) *films* of thickness ranging from 35 μm to 220 μm . The spectra were interpreted numerically on the basis of a model similar to ours, *i.e.* taking into account the strongly inhomogeneous internal field, but the resonance fields (measured for both in-plane and perpendicular configurations) were found to be sensitive to the *film* thickness. This effect is, in fact, not predicted by the results of our study, performed on *cubic-shaped* samples: almost identical local field Ω_n profiles (depicted with bold lines in Fig. 6) were found inside two cubes of different sizes, $2L=40$ and $2L=100$, and moreover, the mode frequency spectrum distribution with respect to Ω_n is almost identical in both cases. Therefore, we may conclude that the above-discussed size-independence of our magnetostatic mode spectrum resulted from the assumed *cubic* shape of the studied sample.

A problem to be solved next is the mode localization behaviour when the sample is „deformed”, losing its cubic symmetry. In our next paper we are going to calculate the magnetostatic mode spectrum in a rectangular finite thin platelet. Our preliminary results indicate that the magnetostatic mode localization effects described here for cubes are present in rectangular platelets as well. We believe, in fact, that this effect is just underlying the so-called ‘bimodal’ statistical distribution of the internal field, recently revealed in finite YIG thin films by Pardavi-Horvath and Yan², and found to be clustered around two major

components – a low-field peak corresponding to the central (volume) part of the sample, and a higher internal field related to the surface – which would correspond exactly to CL and SL modes discussed in this work. Closer elucidation of this analogy will be the subject of our subsequent paper.

Another question requiring future investigation is the mode localization dependence on mode propagation direction. In another study we are going to examine magnetostatic modes propagating *perpendicularly* to the applied field.

Acknowledgments

This work was supported by the Polish Committee for Scientific Research through the projects KBN - 2P03B 120 23 and PBZ-KBN-044/P03-2001.

-
- * Corresponding author: H. Puzkarski, Surface Physics Division, Institute of Physics, Adam Mickiewicz University, ul. Umultowska 85, 61-614 Poznan, Poland; *Email address*: hen-pusz@amu.edu.pl
- ¹ D. Shi, B. Aktas, L. Pust, F. Mikailov (Eds.), *Nanostructural Magnetic Materials and Their Applications*, Lectures notes in physics: Vol. 593; (Springer-Verlag, Berlin 2002).
- ² M. Pardavi-Horvath and Jijin Yan, *IEEE Trans. Magn*, **39** (2003) 3154.
- ³ Toshinobu Yukawa and Kenji Abe, *J. Appl. Phys.* **45** (1974) 3146.
- ⁴ Z. Zhang *et al.*, *Appl. Phys. Lett.* **68** (1996) 2005.
- ⁵ G.P. Berman, F. Borgonovi, Hsi-Sheng Goan, S.A. Gurvitz, and V.I. Tsifrinovich, *Phys. Rev.* **B67** (2003) 094425.
- ⁶ J. Jorzick, S.O. Demokritov, B. Hillebrands, M. Bailleul, C. Fermon, K.Y. Guslienko, A.N. Slavin, O.V. Berkov and N.L. Gorn, *Phys. Rev. Lett.* **88** (2002) 47204.
- ⁷ J.P. Park, P. Eames, D.M. Engebretson, J. Berezovsky and P.A. Crowell, *Phys. Rev. Lett.* **89** (2002) 277201.
- ⁸ D.V. Berkov, N.L. Gorn and P. Görnert, *phys. stat. sol. (a)* **189** (2002) 409.
- ⁹ S. Tamaru, J.A. Bain, R.J.M. van de Veerdonk, T.M. Crawford, M. Covington and M.H. Kryder, *J. Appl. Phys.* **91** (2002) 8034.

- ¹⁰ R. Damon and J. Eshbach, *J. Phys. Chem. Solids* **19** (1961) 308.
- ¹¹ K.Y. Guslienko, R.W. Chantrell and A.N. Slavin, *Phys. Rev. B* **68** (2003) 24422.
- ¹² H.J.G. Draaisma and W.J.M. de Jonge, *J. Appl. Phys.* **64** (1988) 3610.
- ¹³ E.Y. Vedmedenko, H.P. Oepen, J. Kirchner, *J. Magn. Magn. Matter* **256** (2003) 237.
- ¹⁴ G. Gubbiotti *et al.* *J. Appl. Phys.* **93** (2003) 7595 and 7607.
- ¹⁵ L.D. Landau and E.M. Lifshitz, *The Classical Theory of Fields* (Pergamon Press, Oxford, 1975), p. 119.
- ¹⁶ Norberto Majlis, *The Quantum Theory of Magnetism*, World Scientific Publishing Co., Singapore 2000.
- ¹⁷ Y. Zhai, J. Shi, X.Y. Zhang, L. Shi, Y.X. Xu, H.B. Hung, Z.H. Lu and H.R. Zhai, *J. Phys.: Cond. Matter* **14** (2002) 7865
- ¹⁸ Martha Pardavi-Horvath, Bela Keszei, Janos Vandlik and R.D. McMichael, *J. Appl. Phys.* **87** (2000) 4969

FIG. 1: (a) The prism sample considered here; the case in which the applied field, \vec{H}_0 , sets the magnetic moments in the direction perpendicular to the prism base (*i.e.* along the z -axis). The prism 'thickness' is $(N-1)a$, and the square base side width is $2La$ (a denoting the lattice constant). The magnetostatic waves are assumed to propagate along the z -axis (*i.e.* in the direction of the applied field). (b) The planar prism model used in our calculations.

FIG. 2: We consider a cube of edge size $40a$, magnetized uniformly along the z -axis by the applied magnetic field (M_S being the magnetization). Magnetostatic modes are assumed to propagate only in the direction of the applied field. The dipolar field entering the equation of motion is calculated numerically along the central axis (brought into close-up in the graph).

FIG. 4: Numerically calculated magnetostatic mode profiles in a cubic sample of edge size $40a$; the profiles are depicted along the central axis (indicated in Fig. 2) showing separately: (a) the dynamical magnetization m^+ relative values, and (b) the corresponding absolute values, $|m^+|$.

FIG. 5: The modes shown in Fig. 4 are divided here into symmetrical (right column) and antisymmetrical (left column) groups. The modes within each group can be regarded as a family generated by the *bulk-extended* top mode: with lowering mode frequency, the ferromagnetic mode tails shrink, resulting in the appearance of three mode localization types: *central-bulk*, *non-central* and *surface* localization.

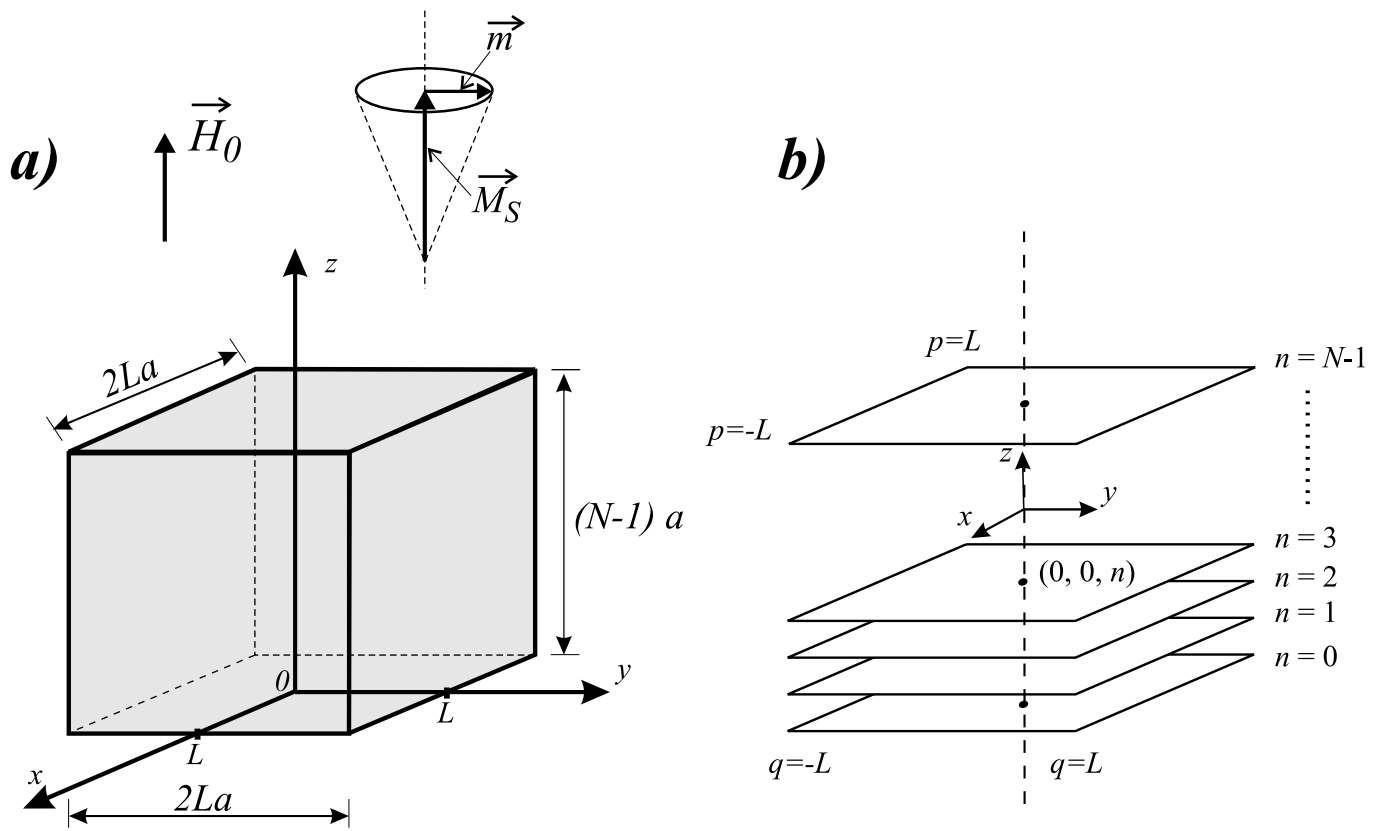
FIG. 3: The quantized magnetostatic mode frequencies *vs.* the cube size, N ; m indicates the mode number.

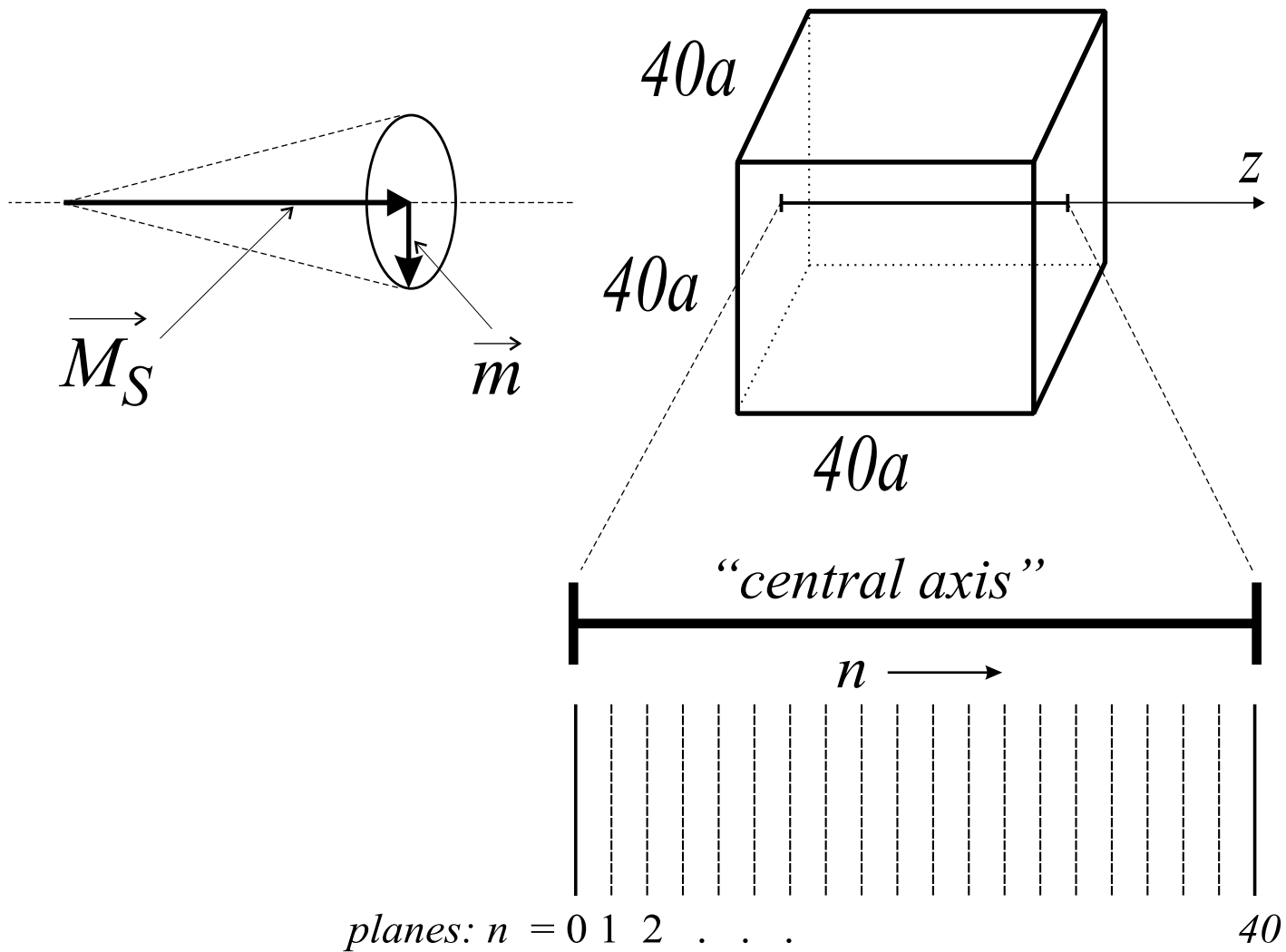
FIG. 6: The quantized magnetostatic mode frequencies (square points) *vs.* the mode number, m ; note the double degeneration of the lower-spectrum modes. Note also that the frequencies of modes $m = N$ and $m = N - 1$ are clearly separated from those of the remaining modes. The bold line represents the spatial distribution of the local dipolar field Ω_n values along the central axis. The cube edge size is (a) $2L = N - 1 = 40$, and (b) $2L = N - 1 = 100$.

FIG. 7: Juxtaposition of magnetostatic mode profiles in two cubes of different sizes. Note that when the cube size increases, the lower modes tend to localize in the surface region, while the upper modes become strongly localized around the cube center; the two highest modes remain practically unchanged.

FIG. 8: An illustration of the size-induced localization effect. When the cube size increases, the localization regions of the localized modes ($m = N-6, 5$ and 1) narrow down substantially.

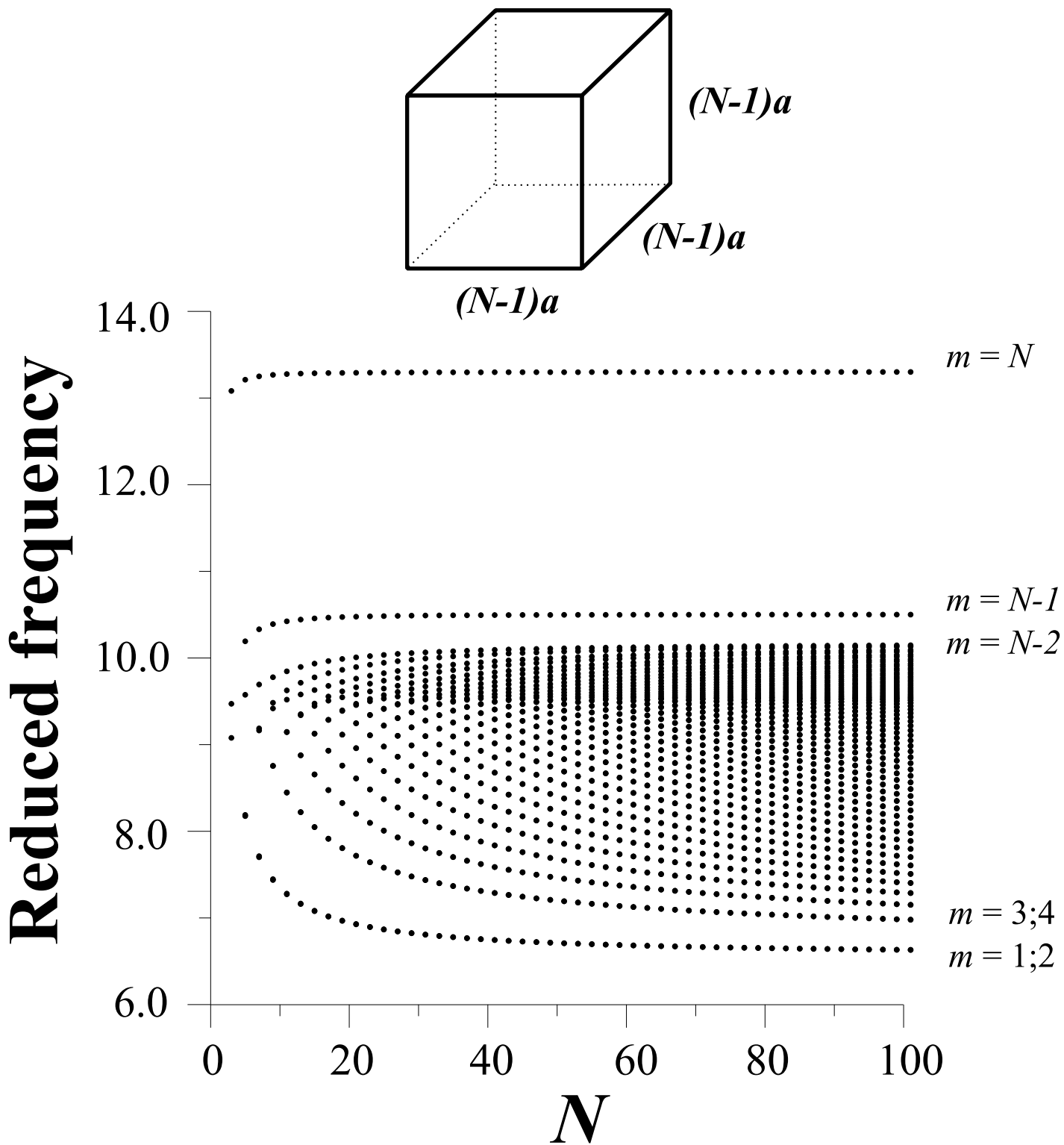
FIG. 9: Magnetostatic mode spectrum in a cube of size $40a$ confronted with the spatial distribution of the local dipolar field Ω_n (bold line) along the cube central axis. A striking feature is that the local field line borders the “empty” region where mode amplitudes are suppressed. The bulk-extended mode frequencies lie *above* the local field range.



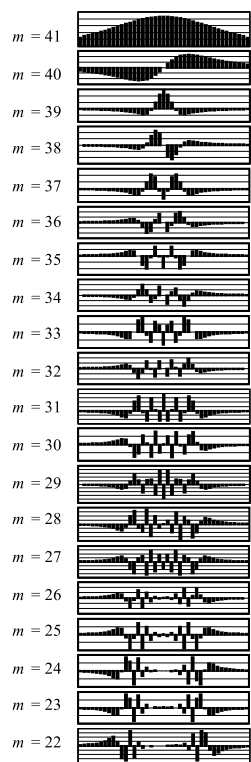
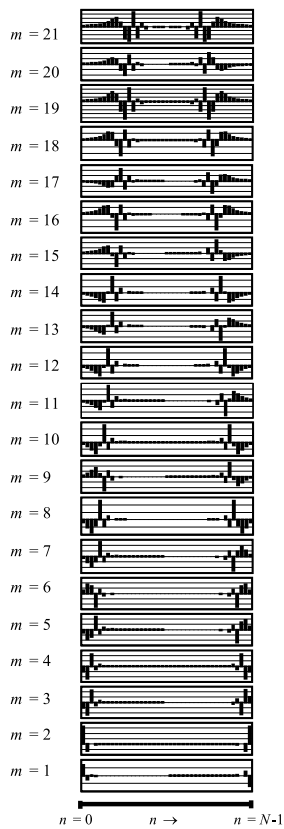


H. Puzkarski, M. Krawczyk and J.-C. S. Levy
 "Localization Properties"

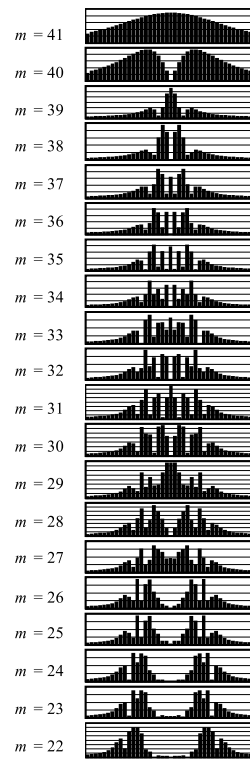
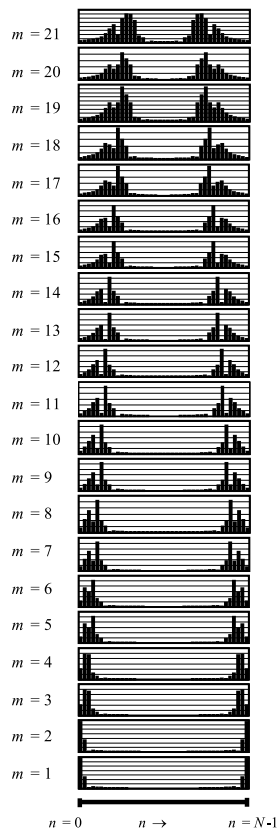
Fig. 2.



(a) $2L=40; N=41$

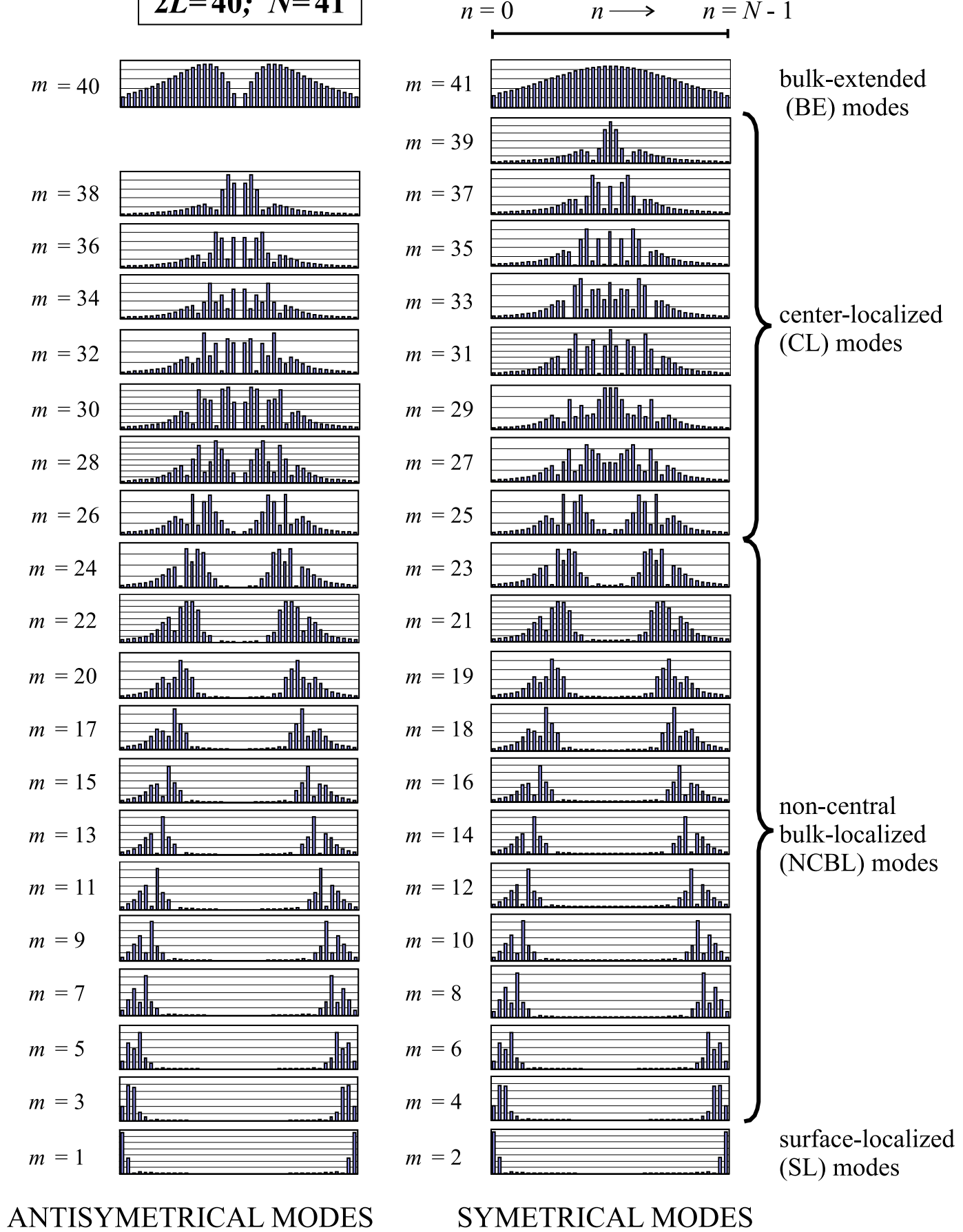


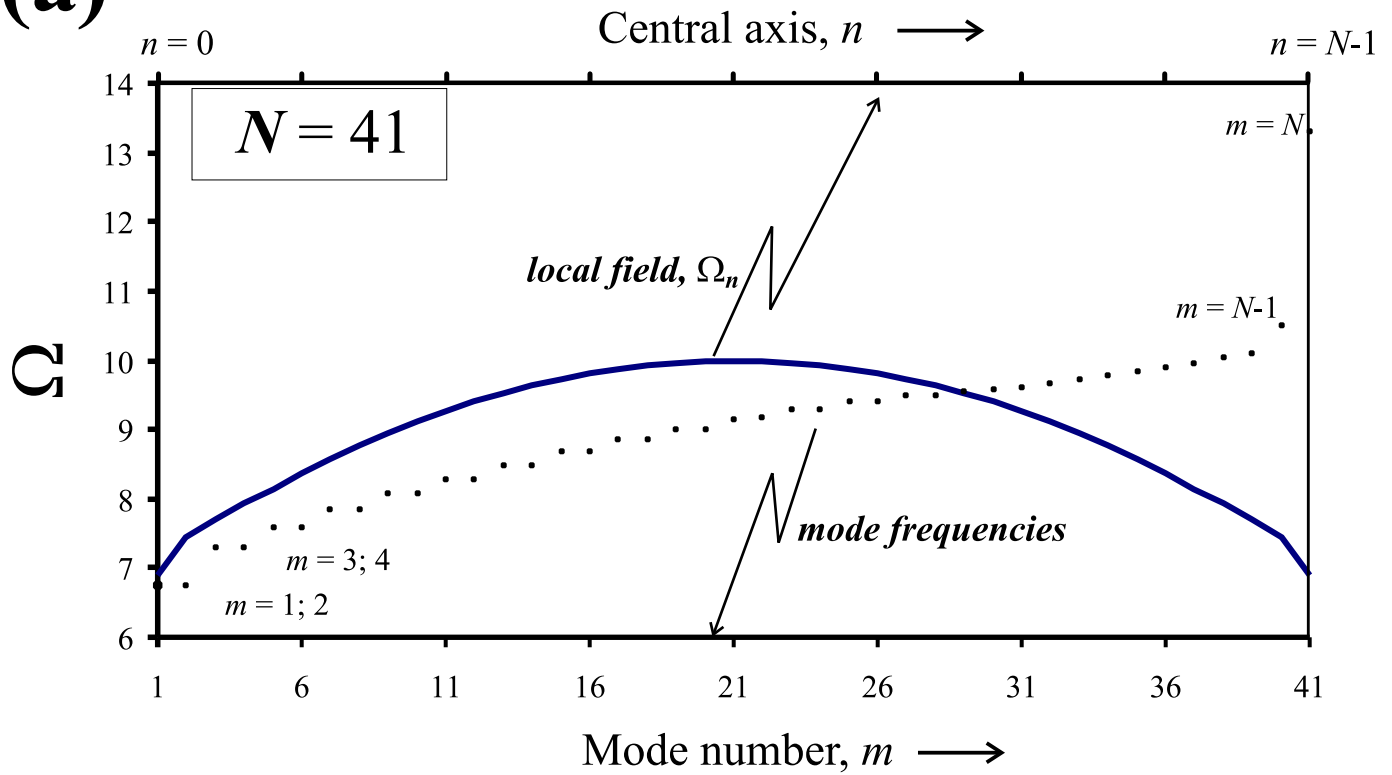
(b) $2L=40; N=41$



H. Puskarski, M. Krawczyk and J.-C. S. Levy
"Localization Properties"

Fig. 4a, b



(a)**(b)**